Available online at www.sciencedirect.com
ScienceDirect
Journal of the European Ceramic Society 28 (2008) 2137–2149
www.elsevier.com/locate/jeurceramsoc

Effect of Ti ion substitution on the structure of hydroxylapatite

Celaletdin Ergun *

Istanbul Technical University, Department of Mechanical Engineering, 34437 Beyoglu, Istanbul, Turkey

Received 17 October 2007; received in revised form 24 February 2008; accepted 6 March 2008
Available online 13 May 2008

Abstract

In order to increase the understanding of the interaction of titanium (Ti) ions with hydroxylapatite (HA) structure, two different kinds of experiments were carried out. In the first, titanium ion containing HA was made via a precipitation method. Tetraethyl orthotitanate were added to precipitating HA to incorporate Ti ions into HA structure. The precipitates were dried and sintered in air at 500 °C, 700 °C, 900 °C, 1100 °C, and 1300 °C for 2 h. X-ray diffraction, Fourier transform infrared spectroscopy, and scanning electron microscopy analysis were used to characterize the samples. In the second, rather as the complementary experiments to the first set, powder mixtures of HA/$CaTiO_3$, tri-calcium phosphate/$CaTiO_3$ were sintered in air at 900 °C, 1100 °C, and 1300 °C for 2 h, and characterized with X-ray diffraction technique. Lattice parameters from X-ray diffraction spectra showed that Ti incorporation into the apatite structure caused lattice shrinkage. The grain sizes of substituted HAs were smaller than those of pure HA. Increasing the amount of the Ti ions in HA caused the decomposition of HA associated with the formation of α-tricalcium phosphate and $CaTiO_3$. This enhanced the porosity in titanium containing HA compared to pure HA. As also verified by the results of complementary experiments, α-tricalcium phosphate (TCP) and $CaTiO_3$ reacted at 1300 °C in the expense of both phases in the presence of HA. No reaction products in the form of new phases could be identified. On the other hand, the same reaction was not observed in the samples that did not have stable HA phase.

Keywords: Apatite; Titanium substitution; Tri-calcium phosphate; Sintering; $CaTiO_3$

1. Introduction

Hydroxylapatite (HA, $Ca_{10}(PO_4)_6(OH)_2$) is a major mineral component of the calcified tissues (i.e. bones and teeth). Synthetic HA has a similar composition and structure to biological apatite. Therefore, it has been safely and extensively used as an implant material for bone substitute with its excellent osteoconductive properties.[1–6] Synthetic HA has been used for various biomedical applications like matrices for drug release control, bone cements, tooth paste additive, monolithic implants or coatings on metallic implants, such as Ti alloys, CoCrMo alloys or stainless steels, etc.[5–8] Non-medical applications of HA include packing media for column chromatography, gas sensors, catalysis and host materials for lasers.[9] Recently, much attention has been focused on nano-crystalline HA as an adsorbent for removing pathogenic proteins from blood for blood purification therapy[10–14] since HA has good blood compatibility as well as a superior ability for selective protein adsorption. The major factors affecting the performance of HA on these applications are crystal morphology, density, porosity, pore size and distribution, chemical composition, and surface structure. These applications stimulate to develop new methods to synthesize HA.

Non-stoichometric HA has a hexagonal space group *P*63/*m* with $a = 0.943$ nm and $c = 0.688$ nm. The unit cell of crystalline HA has 10 cation sites arranged in two non-equivalent positions. Four of them, called Ca(I) sites, are aligned in the column and each surrounded by nine oxygen atoms. Six of them, called Ca(II) sites, are arranged at the apexes of staggered equilateral triangles and each surrounded by seven oxygen atoms. Its structure is characterized by ordering within OH^- ion columns to form a sequence; –OH–OH–OH–OH–. Its (0 0 1) plane consists of columns of skewed 3 Ca(II)–O trigonal prisms around the 6_3 axes. As a distinct feature of its structure, P and O form PO_4 tetrahedras. These tetrahedras do not share the oxygen atoms between themselves and they are rather held together just by the Ca(I) atoms.[15,16] The binding energy of OH^- ions in HA is the lowest. As a result, OH^- ions can escape from HA lattices first if they obtain enough energy in the form of heats or elastic energy due to high lattice strains.[17] Thus HA becomes unstable at high temperatures, caused by dehydration as correlative

* Tel.: +90 505 272 7516; fax: +90 212 245 0795.
E-mail address: ergunce@itu.edu.tr.

0955-2219/$ – see front matter © 2008 Elsevier Ltd. All rights reserved.
doi:10.1016/j.jeurceramsoc.2008.03.007

with the feature of its crystal structure. After the creation of vacancies by the lost of two hydroxyl ions, calcium ions become more weakly bound and can displace which will lead to the further decomposition of HA phase into a more stable calcium phosphate phase.[18]

With its lattice arrangement, HA can be considered a loosely packed hexagonal structure.[19] As provided by the high flexibility of the apatite structure a great variety of cationic and anionic species can be substituted into HA structure which is specifically considered as an effective method to modify the properties of HA. By this way, the volume of the apatite lattice can easily expand and contract, as demonstrated by the formation of many other apatite compounds.[6,20] If the general formula for apatites is $X_{10}(TO_4)_5Z_2$, X can be Ca, Sr, Pb, Cd, and Ba; T can be P, As, and V; Z can be OH, F, and Cl. All these compounds have the same hexagonal structure. Many other divalent cations can substitute for calcium ions in the structure of HA; larger ions than calcium cause an expansion of the structure and smaller ions a contraction.[21] Moreover, rare-earth ions can also substitute in the apatite structure, leading to changes in its refractive index and lattice parameters of the apatite crystals.[22]

HA in composites can be made more resistant to high temperature decomposition by substituting small amounts of impurities in the HA phase, such as, $Na^+/(CO_3)^{2-}$, $Mg^{2+}/(CO_3)^{2-}$, CaO^+, F^-.[23–29] The low amount of Ag^+, Cu^{2+}, Zn^{2+} substitution into HA structure has a potential of minimizing the risk of bacterial contamination, without compromising the bioactivity, and is expected to display greater biological efficacy in terms of osseointegration.[30–32] Si substitution increased the chemical stability and bioactivity of hydroxylapatite.[33,34] Carbonated-HA had a high blood compatibility and selective adsorption of pathogenic proteins, such as b2-microglobulin (b2-MG).[12] Substituting the Zn^{2+} ions for the Ca^{2+} ions in HA resulted in selective adsorption of physiologically active components in blood.[35] Finally, enhanced osteoblast adhesion was observed on Y^{3+}-doped HA.[36] There have been also many other studies on HAs substituted with various ions such as Cr^{3+}, Fe^{3+}, Al^{3+}, La^{3+}, Eu^{2+}, Ce^{2+} to document their various materials proprieties.[37–41]

Interaction of HA with titanium ions was indirectly performed at the HA–Ti interface of the HA coatings on the Ti substrates. Mutual diffusion of elemental Ti and the ions in HA across the interface was observed which might be considered as an evidence for the incorporation of Ti into HA structure.[42] As one of a few studies focusing directly on Ti incorporation into HA, Wakamura et al. reported that hydroxylapatite modified with Ti^{4+} ions exhibited very good photocatalytic activity in oxidation and decomposition of acetaldehyde.[43] This effect makes possible to use them in untibacterial applications.[44,45] Ribeiro et al. made structural examination on the Ti substituted HA. They reported that Ti ions incorporated into Ca sites in the HA lattice.[46] In another study, osteoblast adhesion on Ti substituted HA showed an appreciable increase when compared to pure HA.[47]

Not much studies have been found in the literature on the effect of Ti ions on the structure of HA and its structural stability during processing at high temperatures. The objective of the current study is to develop a better understanding on the structure and behavior of the Ti incorporated HA. In order to do this, two sets of samples were synthesized and characterized. In the first, Ti-doped HA was made by a precipitation method, and sintered in air between 500 °C and 1300 °C. Subsequently, the materials were characterized by X-ray diffraction (XRD), Fourier transform-infrared spectroscopy (FT-IR), scanning electron microscopy (SEM) equipped with EDS, and density measurements. In the second, the HA/$CaTiO_3$ and tricalcium phosphate (TCP)/$CaTiO_3$ composites were prepared and sintered in air between 900 °C and 1300 °C. Then they were characterized with X-ray diffraction method.

2. Materials and methods

2.1. Synthesis of titanium-substituted apatites

Pure HA, TCP-whitlocite, and Ti-doped HA were synthesized with precipitation method.[21] Briefly, for pure HA synthesis, solutions of 1 M $Ca(NO_3)_2{\cdot}4H_2O$ and 0.6 M $(NH_4)HPO_4$ were separately brought to pH 11–12 with concentrated NH_4OH. The calcium nitrate solution was stirred vigorously at room temperature (RT), and the ammonium phosphate solution was added dropwise into this calcium nitrate solution to produce a gelatinous precipitate. The precipitated solution was stirred for 24 h at RT to form nano-grained HA. For pure TCP synthesis, first, the 1.5 M $Ca(NO_3)_2{\cdot}4H_2O$ (Fisher Scientific, 99% pure) and 1 M $(NH_4)HPO_4$ (Fisher Scientific, 98% pure) were separately brought to pH 11–12 with concentrated NH_4OH. The same steps as those used for HA synthesis were applied to get nano-grained powder. Then, a heat treatment at 1100 °C for 1 h was carried out to transform the precipitate powders into TCP.

Reagent grade tetraethyl orthotitanate ($C_8H_{20}O_4Ti$) (Fulka, 20% Ti) was added into the calcium nitrate solution to synthesis the Ti substituted HA. Ti molar incorporation ratios for Ca or P ions were chosen as 2 mol% or 5 mol%. The stoichometric value of 1.67 for (Ca + Ti)/P or Ca/(P + Ti) ratio was aimed to achieve in the HA after incorporation of Ti ions into Ca or P sites. Therefore, molar ratios of Ca or P ions deliberately added 2 mol% or 5 mol% less than that of required for pure HA into the precursor solutions in order to compensate the difference with Ti ions. In other words, for 2 mol% or 5 mol% Ti substitution into Ca positions, solutions of 0.98 M or 0.95 M $Ca(NO_3)_2{\cdot}4H_2O$, respectively, were used, while $(NH_4)HPO_4$ solution was 0.6 M. For 2 mol% or 5 mol% Ti substitution into P positions, solutions of 0.58 M or 0.55 M $(NH_4)HPO_4$, respectively, were used, while $Ca(NO_3)_2{\cdot}4H_2O$ solution was 1 M. The reaction mixture was centrifuged and washed repeatedly to remove the unreacted ammonia. Next, the sludge was filtered using a 0.2-μm filter paper to form a sticky cake, which was then dried for at least 48 h at 60 °C. Dried cakes were crushed and passed through a 200-mesh screen to obtain a powder with particle sizes <75 μm in diameter.

Reagent grade $CaTiO_3$ powders were purchased from a commercial supplier (Alfa Aesar, 99% pure). The synthesized powders of HA and TCP were mixed with $CaTiO_3$ to obtain the desired weight ratios. The description and the composition of

Table 1
Abbreviation and composition of the compacts tested in the present study

Compact	Abbreviation	Composition
Hydroxylapatite	HA	Pure
Tricalcium phosphate	TCP	Pure
Hydroxyapatite doped with Ti	C2 C5 P2 P5	Refer to Table 2
Calcium titanate ($CaTiO_3$)	CT	100%
Hydroxyapatite:calcium titanate composites	HC	70 wt.% HA + 30 wt.% $CaTiO_3$
Tricalcium phosphate:calcium titanate composites	TC	70 wt.% TCP + 30 wt.% $CaTiO_3$

the samples are shown in Table 1. For homogeneous mixing, the powders were blended by ball milling (Retsch PM100) in an ethyl alcohol medium. The milled powder was then quickly filtered through a 0.2-μm Millipore filter to prevent segregation due to density differences between the two types of powders. The filtered cakes were kept at 200 °C overnight. The cakes were then crushed and further mixed using a pestle and mortar.

The powders of pure and substituted apatites and composites containing $CaTiO_3$ were cold-pressed into cylindrical pellets under 150 MPa pressure. Resulting pellets were about 1 cm in diameter and 3 mm in thickness. Subsequently, the pellets were sintered in air at 500 °C, 700 °C, 900 °C, 1100 °C, and 1300 °C for 2 h depending on the experimental protocol.

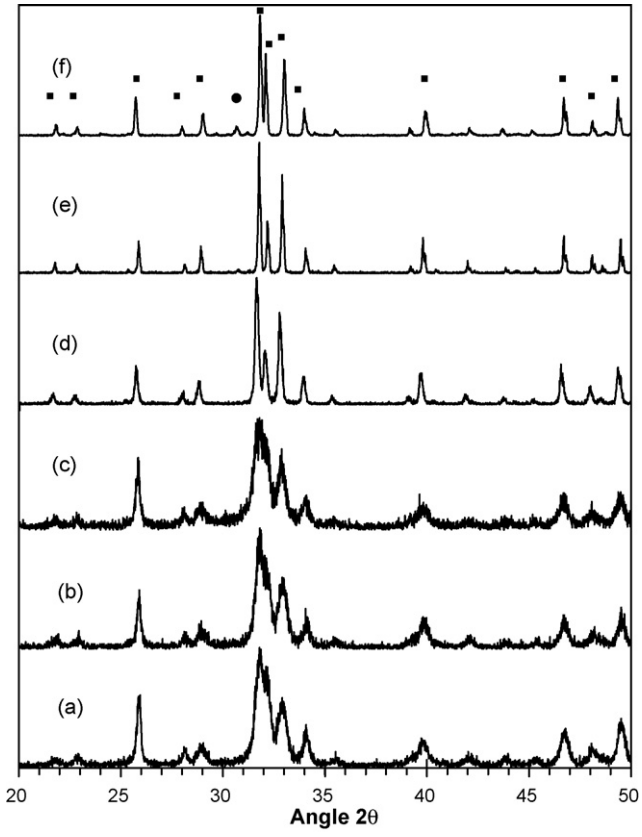

Fig. 1. XRD patterns of air-sintered HA samples: (a) as precipitated; and sintered for 2 h at: (b) 500 °C; (c) 700 °C; (d) 900 °C; (e) 1100 °C; (f) 1300 °C. (■) Hydroxylapatite; (●) α-tricalcium phosphate). *Y*-axis, arbitrary units.

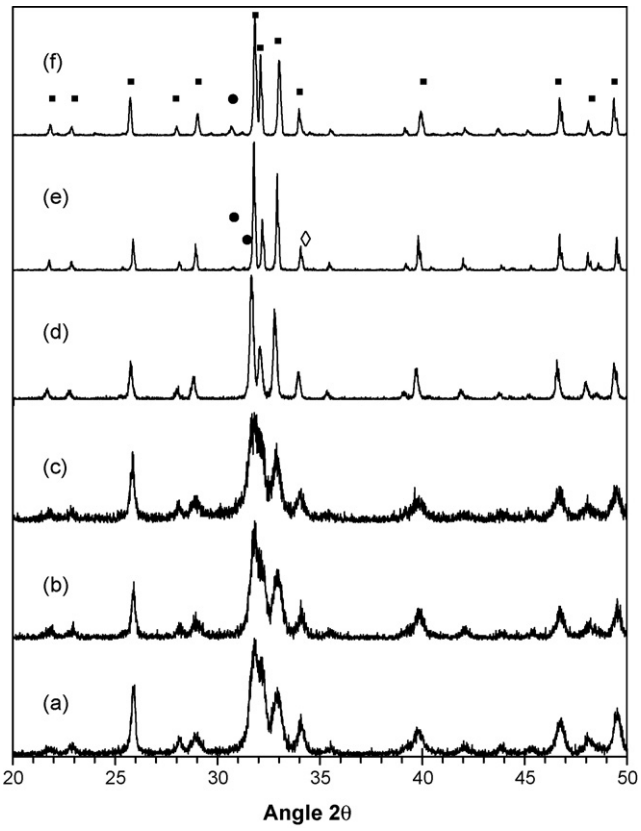

Fig. 2. XRD patterns of air-sintered C2 samples: (a) as precipitated; and sintered for 2 h at: (b) 500 °C; (c) 700 °C; (d) 900 °C; (e) 1100 °C; (f) 1300 °C. (■) Hydroxylapatite; (●) α-tricalcium phosphate; (◊) calcium titanate. *Y*-axis, arbitrary units.

After sintering, one surface of each pellet was polished with SiC paper and then with diamond powder. The surfaces were finished with a 0–1-μm diamond solution.

2.2. Materials characterization

Lattice parameters (*a* and *c*) and phases present in the HA were determined with X-ray diffraction (using a Philips type PW2273/20 diffractometer). The structure of HA is usually considered to be hexagonal, with space group *P*63/*m*. However, there is evidence for a variant HA structure that is monoclinic, with atomic positions that are close to those of the hexagonal structure. For our present purpose, we will consider the structure of HA to be hexagonal for lattice parameter measurements.

Cu Kα radiation (λ = 1.5406 nm) produced at 40 kV and 35 mA scanned the diffraction angles (2*θ*) between 20° and 70° at every 0.02° for 20 s. Diffraction signal intensity throughout the scan was monitored and processed with JADE software. Changes were calculated by subtracting the values of lattice parameters *a* and *c* of undoped from doped HA formulations.

FTIR spectra of sample powders were recorded at room temperature on a PerkinElmer Fourier transform-infrared spectrometer using an ATR attachment. Grain size and porosity of

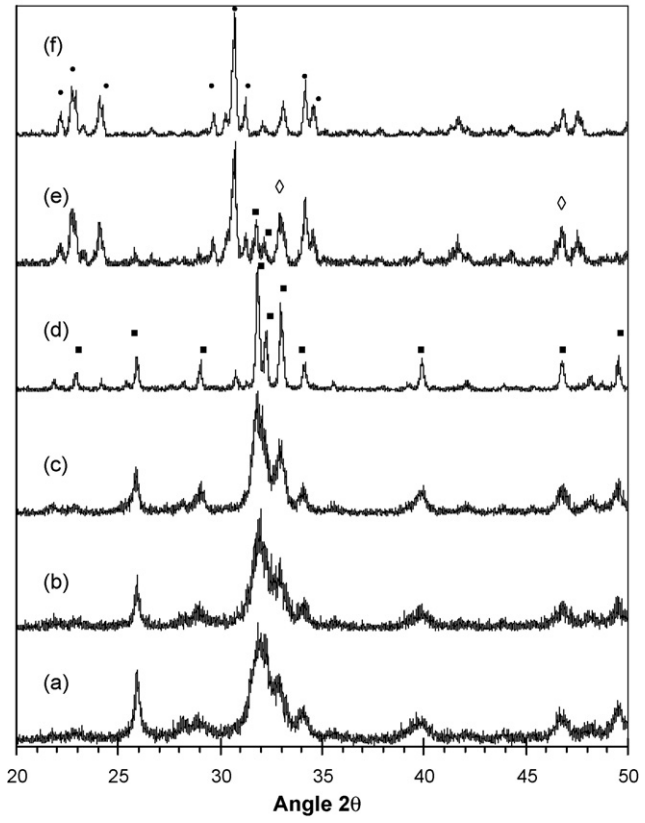

Fig. 3. XRD patterns of air-sintered C5 samples: (a) as precipitated and sintered for 2 h at: (b) 500 °C; (c) 700 °C; (d) 900 °C; (e) 1100 °C; (f) 1300 °C. (■) Hydroxylapatite; (●) α-tricalcium phosphate; (◊) calcium titanate. *Y*-axis, arbitrary units.

the pure and substituted hydroxylapatite samples of this study were determined by SEM (Philips/FEI XL30FEG SEM Electron Microscope system). For the examination of the HA under SEM, it was etched in a 0.1-M lactic acid (Sigma) and coated with gold at RT. Samples were examined at 20 kV. Linear intercept method was used to determine the average grain size.[48,49] Chemical analyses were performed on the samples sintered at 1100 °C for 2 h with the same SEM system in conjunction with the energy dispersive spectrometer.

The relative concentrations of the different phases were determined by the following equation[50]:

$$\mathrm{RC}_i = \frac{I(h\,k\,l)_i}{\sum I(h\,k\,l)_i} \quad (1)$$

where i, RC_i, and $I(h\,k\,l)_\mathrm{i}$ refer to the phase in interest, relative concentration of the corresponding phase, and intensity of the characteristic peaks of the corresponding phase, respectively, in the XRD patterns. Peaks belonging to (2 1 1) plane for HA, (1 7 0) plane for α-TCP, (1 2 1) plane for CT were used as characteristic peaks. $\Sigma I(h\,k\,l)_i$ is the total intensity of the characteristic peaks of the phases appeared in the XRD patterns. Relative concentration is not an absolute value of the concentration of the respected phase that appeared in the materials. However, it is a useful tool to make qualitative evaluation of the phase interactions and reactions occurring during the processes.

The volume (V) of a hexagonal unit cell was determined for each HA from the formula $V = 2.589a^2c$.

The densities of cylindrical samples were calculated from their measured dimensions and mass. A parameter defined as densification factor was used to monitor the density changes of the Ti substituted samples during sintering at different temperatures. This factor was calculated with the following equation:

$$\text{densification factor} = \frac{D - D_\mathrm{g}}{D_\mathrm{g}} \times 100 \quad (2)$$

where D is the density of the sintered compact and D_g is the density of the green compact.

3. Results

XRD patterns of pure HAs are presented in Fig. 1. X-ray peaks of as precipitated phase matches to the JCPDS standard peaks of pure hydroxylapatite. The wide peaks should be due to very small size of the precipitates and/or partial disorderness in the precipitates. This phase became fully crystallized in between 700 °C and 900 °C indicated with the sharp HA peaks. Slight decomposition of the HA to TCP was observed at 1100 °C. The amount of TCP slightly increased at 1300 °C.

XRD patterns of Ti substituted HAs (C2, C5, P2, and P5) are given in Figs. 2–5. Similar to the pure HA, in all Ti substituted samples; the precipitated phase was HA with very small crystallites and/or in disordered state. The precipitates

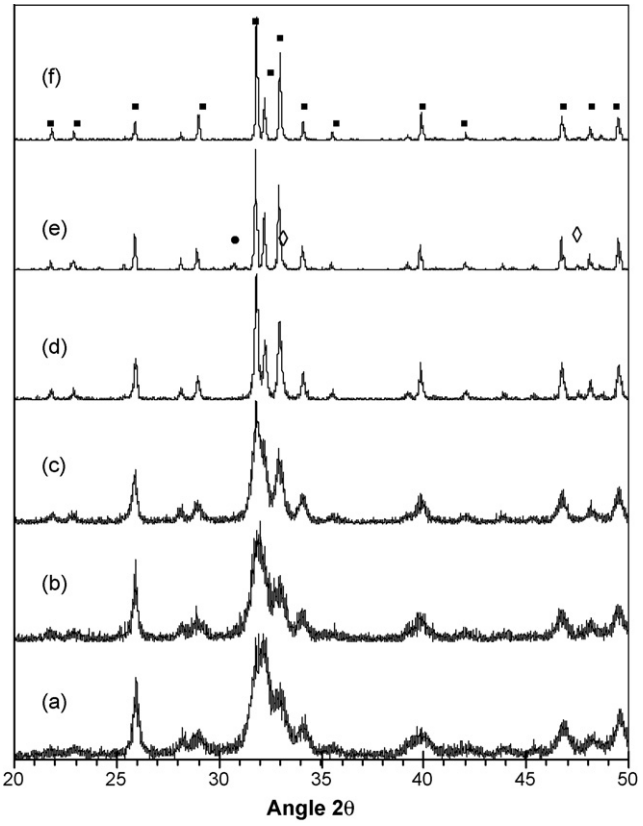

Fig. 4. XRD patterns of air-sintered P2 samples: (a) as precipitated; and sintered for 2 h at: (b) 500 °C; (c) 700 °C; (d) 900 °C; (e) 1100 °C; (f) 1300 °C. (■) Hydroxylapatite and (●) α-tricalcium phosphate. *Y*-axis, arbitrary units.

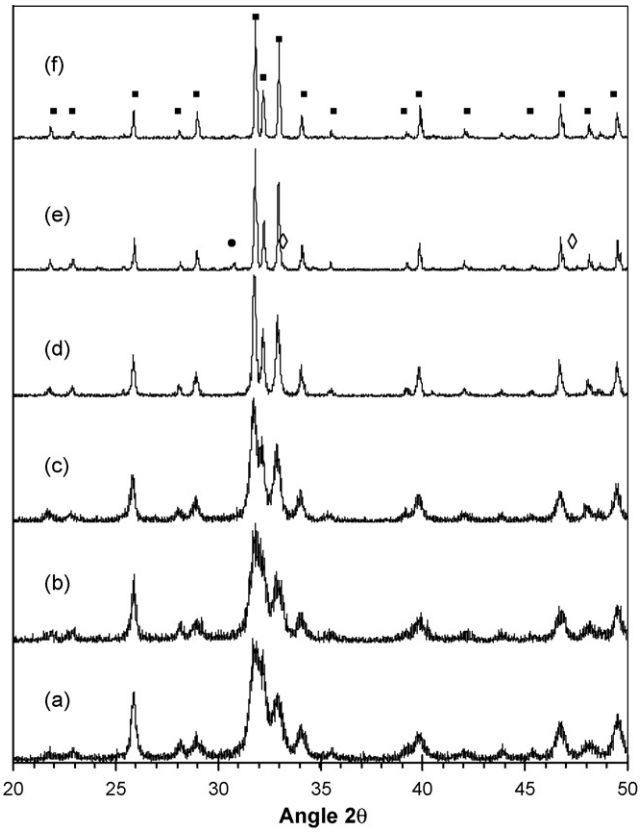

Fig. 5. XRD patterns of air-sintered P5 samples: (a) as precipitated; and sintered for 2 h at: (b) 500 °C; (c) 700 °C; (d) 900 °C; (e) 1100 °C; (f) 1300 °C. (■) Hydroxylapatite and (●) α-tricalcium phosphate. *Y*-axis, arbitrary units.

were fully crystallized after sintering in between 700 °C and 900 °C.

In C2 (Fig. 2), the dominant phase was HA in all sintering conditions. However, α-$Ca_3(PO_4)_2$ (α-TCP) and $CaTiO_3$ phases started to appear at 1100 °C and then α-TCP considerably decreased at 1300 °C, while $CaTiO_3$ phase completely disappeared. In C5 (Fig. 3), HA was not stable at above 900 °C. It was mainly transformed to α-TCP at 1100 °C. It completely disappeared at 1300 °C, while α-TCP became the only stable calcium phosphate phase. $CaTiO_3$ stayed stable at both 1100 °C and 1300 °C.

In P2 and P5 (Figs. 4 and 5, respectively) as similar to C2, the major phase was HA with small amounts of α-TCP and $CaTiO_3$ at 1100 °C. However the amount of both α-TCP and $CaTiO_3$ phases considerable decreased at 1300 °C and the HA remained as the major phase.

The relative XRD peak heights are plotted as a function of sintering temperatures in Figs. 6–9 to compare the phases in the Ti containing samples; C2, C5, P2, and P5. The relative peak heights showed the changes in the amounts of a particular phase but they were not normalized to give absolute concentrations.

In all samples, the precipitated phase (HA with small crystal size), as the starting material, was stable up to 700 °C and began to transform to other phases in between 700 °C and 900 °C. In C2 in Fig. 6, the precipitates formed well-crystallized HA and α-TCP phases at 900 °C. $CaTiO_3$ became apparent at 1100 °C.

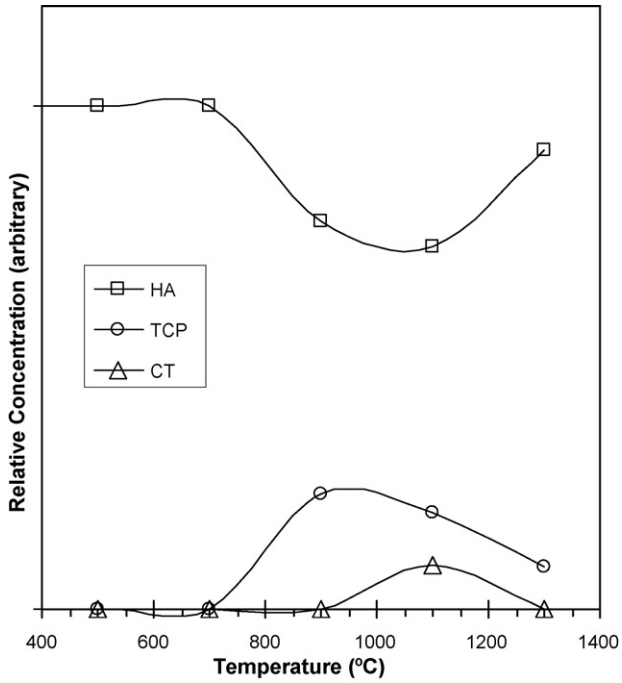

Fig. 6. The change in the relative concentrations of the HA, TCP, and CT in C2 during sintering.

Interestingly, α-TCP phase showed a decrease at 1300 °C while $CaTiO_3$ phase completely disappeared, suggesting a possible reaction between these two phases. In C5, HA totally disappeared between 1100 °C and 1300 °C, α-TCP became the only stable calcium phosphate phase associated with $CaTiO_3$ (Fig. 7). The phase distributions in P2 and P5 throughout sintering up to

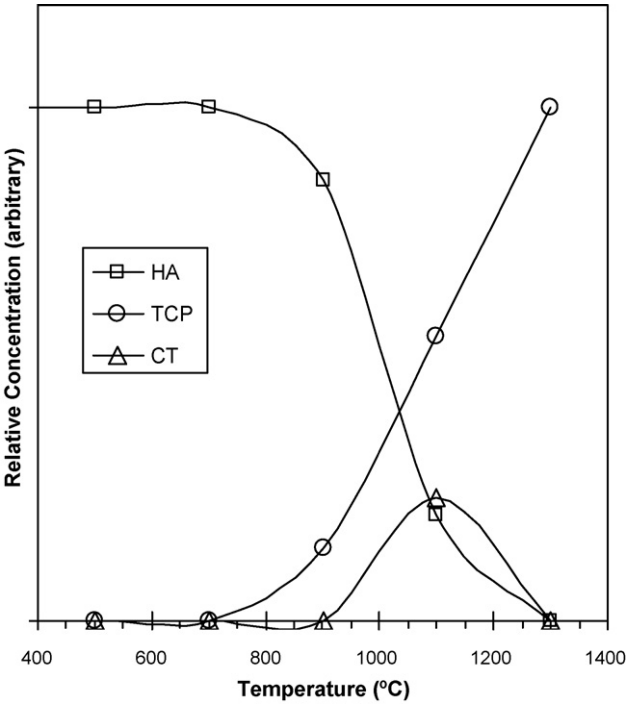

Fig. 7. The change in the relative concentrations of the HA, TCP, and CT in C5 during sintering.

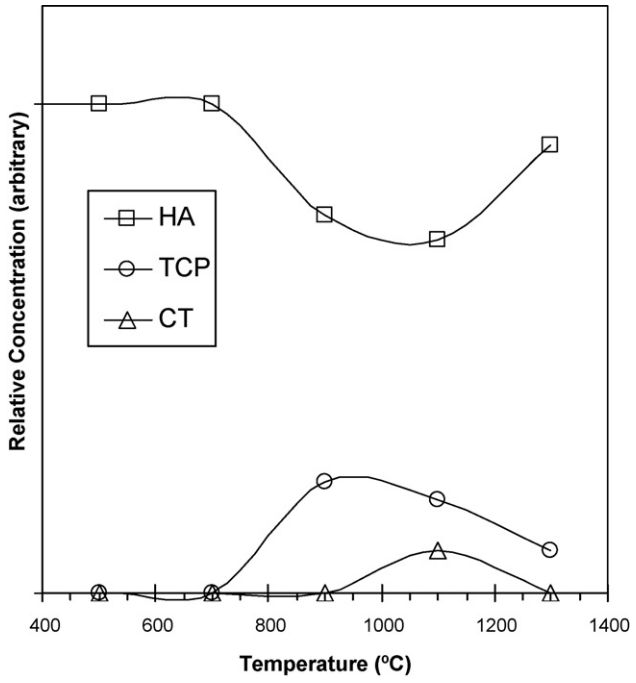

Fig. 8. The change in the relative concentrations of the HA, TCP, and CT in P2 during sintering.

1300 °C were very similar to C2 as presented in Figs. 8 and 9, respectively.

As given in Table 2, Ti concentration was the highest in C5 and it was followed by P2, C2 and P5, respectively. However, the amount of α-TCP in the samples sintered at 1300 °C was the highest in C5 and the lowest in P5. Although it is almost

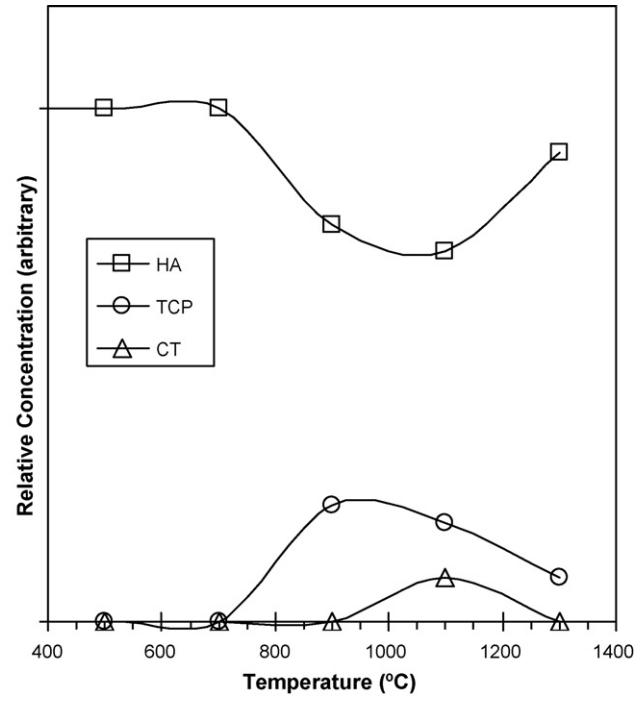

Fig. 9. The change in the relative concentrations of the HA, TCP, and CT in P5 during sintering.

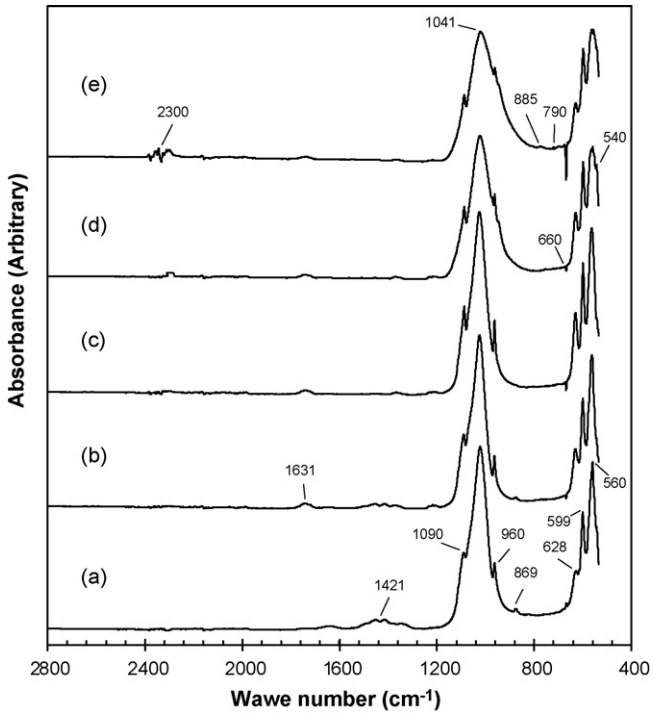

Fig. 10. FTIR spectra of the C2 sintered at: (a) 500 °C; (b) 700 °C; (c) 900 °C; (d) 1100 °C; (e) 1300 °C.

completely disappeared in P2, slight amount of α-TCP was remained in C2. These results showed a correlation between enhancement in the stability of α-TCP phase and increasing Ti ion concentration.

The FT-IR spectrum of C2 presented in Fig. 10 showed that as the sintering temperature increased, the O–H stretching band[45,46] observed at 628 cm^{-1} showed an increase up to 700 °C, which may be due to the increase in crystallinity. However, this band showed a progressive decrease with further increasing the sintering temperature, which may be due to the incorporation of Ti ions into maturing HA crystal structure and/or the dehydration of the structural water. The broad band with low intensity at 1631 cm^{-1} is due to the presence of lattice water in HA structure.[45,46]

The bands at 1090 cm^{-1}, 1041 cm^{-1}, 599 cm^{-1}, 960 cm^{-1}, and 560 cm^{-1} were assigned to PO_4^{3-} stretching.[45,46] There was a broadening of the band at 1041 cm^{-1} with increasing sintering temperature. Moreover, the band at 960 first increased their intensity up to 900 °C, which may be due to the increasing crystallinity. Subsequently, this peak showed a progressive decrease that may be associated with a decrease in crystallinity

Table 2
Composition of pure and doped samples in atomic percentage

Sample reference	Ca	P	O	Ti
C2	42.37	22.95	33.51	1.17
C5	34.48	21.06	41.42	3.04
P2	39.15	23.04	36.57	1.24
P5	30.38	20.52	48.21	0.89
HA	31.22	18.42	50.27	0
TCP	27.88	19.34	52.78	0

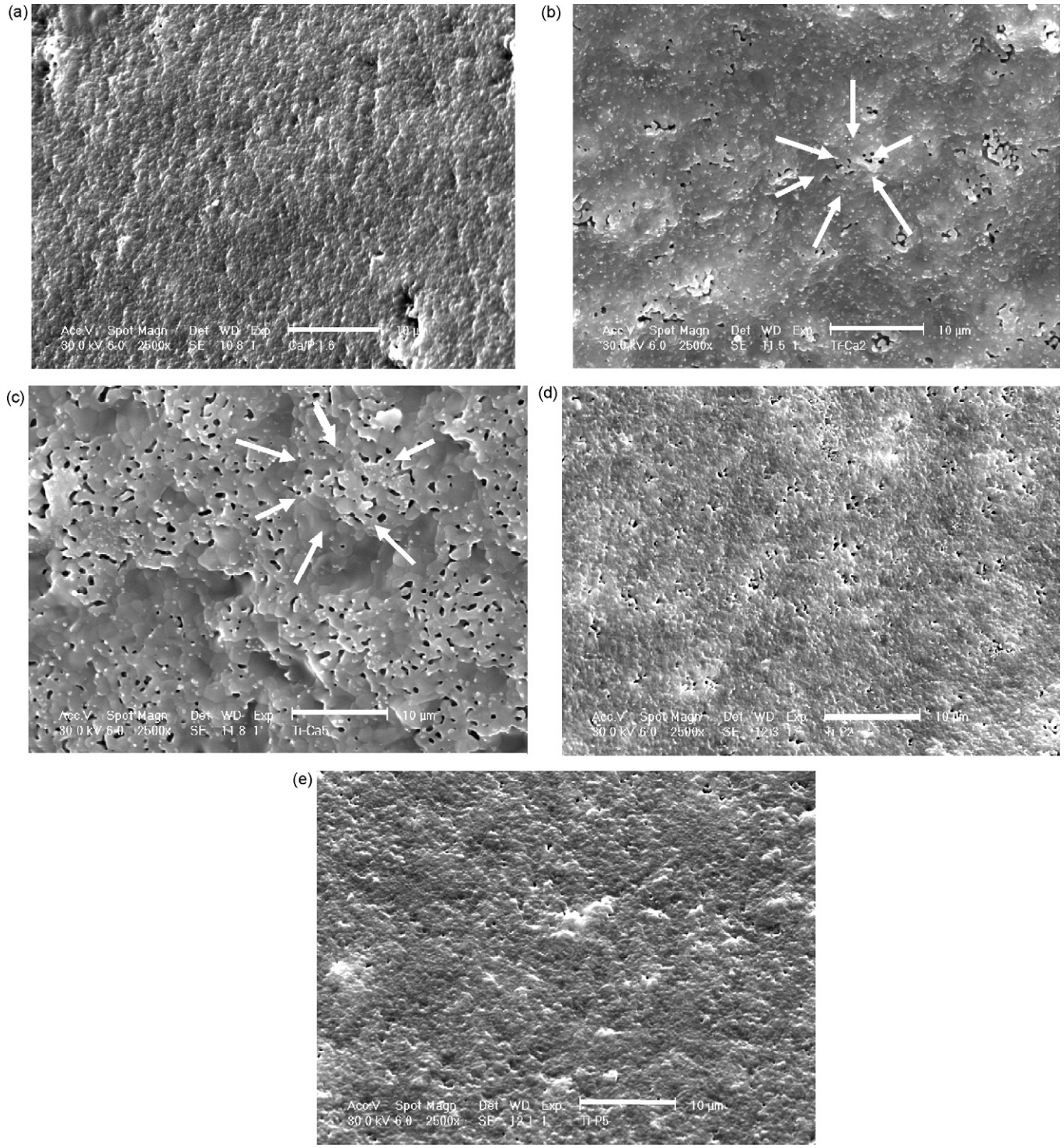

Fig. 11. SEM photographs of Ti-doped HAs sintered at 1100 °C: (a) HA; (b) C2; (c) C5; (d) P2; (e) P5 (arrows show the pores formed during dehydration of HA) (bars = 10 μm).

due to a decrease in crystallite size and increase in lattice imperfection or a combination of these effects in a similar manner observed in O–H band at 628 cm^{-1}. A shoulder at 540 cm^{-1}, which is the characteristic band of TCP, started to appear at 1100 °C, corresponding closely with XRD results given in Fig. 2.

The band at 660 cm^{-1} was observed in all sintering conditions, which is not a characteristic band of pure HA. The intensity of this peak showed a progressive increase up to 1300 °C. New bands at 790 cm^{-1}, 885 cm^{-1}, and 2300 cm^{-1} also became apparent at 1300 °C, which should also associate with the presence of Ti ions in HA structure.

Results of SEM studies showed that HA was highly densified (99.5%) when sintered at 1100 °C for 2 h (Fig. 11(a)). The average grain size of HA was 480 nm. The average grain sizes of

C2, C5, P2 and P5 were 355 nm, 1600 nm, 403 nm, and 330 nm, respectively, after sintering at 1100 °C for 2 h. In contrast, Ti-doped HA samples had significant porosity (Fig. 11(b)–(e)). Specifically, C5 had the highest (52%) amount of porosity followed by C2 (33%) and P2 (18%) with the next highest porosity. P5 (4%) had the lowest amount of porosity among the HA doped with Ti formulations.

The densification factor of the samples calculated with Eq. (1) is given in Fig. 12. In a general trend, density of the samples showed a decrease up to 700 °C most probably due to the lost structural water from the dissociating HA. It subsequently showed a continuous increase with increasing temperature most probably because of the volume shrinkage during sintering. The density was always smallest in C5 while P5 had the highest density which was followed by those of P2 and C2, respectively. The porosity levels were also in this order.

XRD patterns of HC samples demonstrated a small amount of β-TCP (β-$Ca_3(PO_4)_2$) formation at 1100 °C most probably due to the slight dissociation of HA (Fig. 13). However, this phase disappeared upon sintering at 1300 °C, corroborating the results observed in C2, P2 and, P5. On the other hand, the XRD patterns for TC composites showed that α-TCP and $CaTiO_3$ phases did not react and stayed stable at 1100 °C in the absence of HA phase (Fig. 14).

4. Discussion

The results of X-ray analysis of pure and Ti-doped samples showed that the precipitating phase was always HA with very small grain size. However, as the sintering temperature increased above 900 °C, increased crystallization and/or phase transformation in the precipitates were observed. In C2, P2, and P5, $CaTiO_3$ formation and stabilization of α-TCP were monitored at 1100 °C. These results suggested that increasing Ti ion addition beyond a certain solubility limit of the HA structure leads to $CaTiO_3$ formation and stabilization of α-TCP in Ti-doped samples. According to the Ribeiro et al. this solubility limit of Ti ions in the HA lattice is less than 200 ppm.[46] Sintering in between 1100 °C and 1300 °C seemed to cause a reaction involving $CaTiO_3$ and α-TCP in the expense of both phases.

On the other hand, although the precipitated phase formed crystallized HA with small amount of α-TCP phase at 900 °C in C5 as similar to other doped samples, HA was not stable at higher temperatures. The amount of HA considerably decreased at 1100 °C and entirely transformed to α-TCP at 1300 °C. Unlike to C2, P2 or P5, $CaTiO_3$ did not react with α-TCP phase in C5. Based on these results, Ti ion can be considered as an α-TCP stabilizing agent in HA.

Careful inspection of the XRD data of C2, P2, and P5 samples sintered above 900 °C revealed that there were two different superimposed XRD patterns of two different kinds of apatitic structures. The superimposed XRD patterns for P5 sintered at 1100 °C and 1300 °C are given in Fig. 15. These may be due to the two different precipitation mechanisms. The pattern with higher intensity may belong to a Ti ion substituted HA lattice while the other one with lower intensity may belong to a kind of Ti dominant apatitic structure. The hexagonal lattice parameters

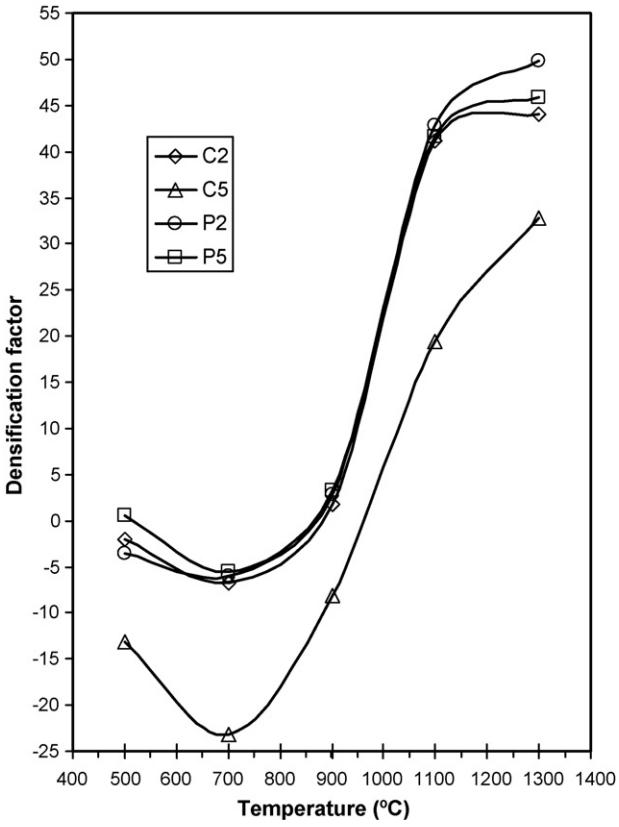

Fig. 12. Densification factor of C2, C5, P2, and P5.

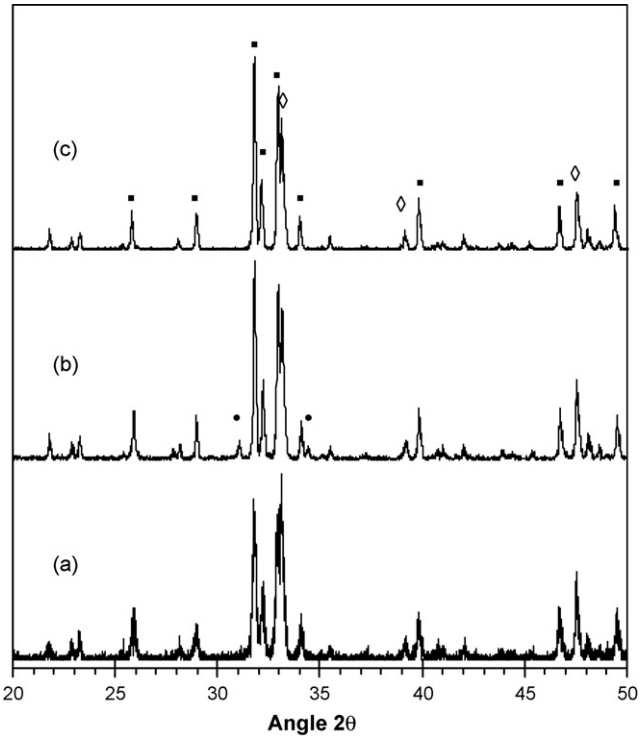

Fig. 13. XRD patterns of HC sintered at: (a) 900 °C; (b) 1100 °C; (c) 1300 °C. (●) α-TCP (β-$Ca_3(PO_4)_6$; (■) HA; (◊) CT. *Y*-axis, arbitrary units.

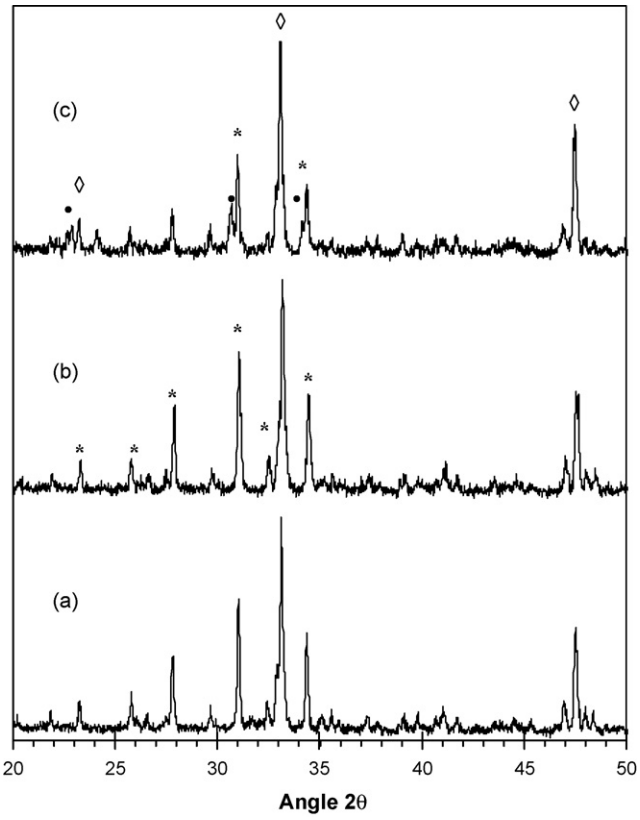

Fig. 14. XRD patterns of TC sintered at: (a) 900 °C; (b) 1100 °C; (c) 1300 °C. (*) β-TCP (β-$Ca_3(PO_4)_6$; (●) α-TCP (β-$Ca_3(PO_4)_6$); (◊) CT. *Y*-axis, arbitrary units.

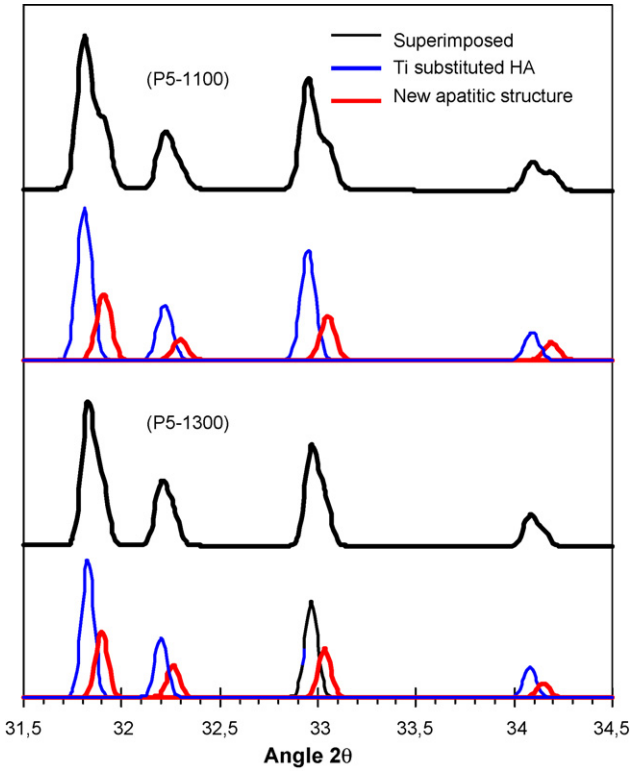

Fig. 15. X-ray diffraction patterns of P5 sintered at 1100 °C and 1300 °C. *Y*-axis, arbitrary units.

were calculated based on these two superimposed XRD patterns (Table 3).

In all substituted apatites, both lattice parameters *a* and *c* in hexagonal structures for both superimposed data were smaller than in pure HA as shown in Table 3. This implies that the HA structure shrank in volume with increasing the amount of Ti. Since the ionic radii of Ti is smaller than that of all components of HA: Ca, O, and P, it is plausible to admit that the substitution of Ti resulted in a shrinkage of the apatite lattice volume. This finding is in agreement with the result reported by Riberio et al.[46] They also reported that the lattice parameters *a* and *c* decreased with increasing the Ti concentration. This suggests that more Ti ions substituted in HA lattice in C2 than P2 and P5.

The FT-IR results in Fig. 10 shows a clear evidence for the strong structural changes in HA lattice upon substituting with Ti ions. A typical structure of HA is characterized by different vibration modes of the phosphate $(PO_4)^{3-}$ and hydroxyl $(OH)^-$ groups. The phosphate group itself has a Td symmetry; resulting in four internal modes (symmetric stretch ν_1, 958 cm^{-1}; asymmetric stretch ν_2, 430–460 cm^{-1}; bending ν_4, 1041–1090 cm^{-1}; bending ν_5, 575–610 cm^{-1}). The bands at 1090 cm^{-1}, 1041 cm^{-1}, 960 cm^{-1}, 599 cm^{-1}, and 560 cm^{-1} were therefore assigned to PO_4^{3-} stretching.

On the other hand, hydroxyl group with $C_{\infty v}$ has vibration modes at frequencies of 3570 cm^{-1} and 628 cm^{-1}. Since the hydroxyl group is located slightly above or below the mirror plane, reducing the molecular symmetry, all four $(PO_4)^{3-}$ absorptions become FTIR active.[51,52] Especially the band observed at 628 cm^{-1} due to O–H stretching was found to be sensitive to substitution in the apatite structure.[46] The strength of this band also shows the degree of crystallinity.

As observed in Fig. 10, an increase in the O–H stretching band at 628 cm^{-1} up to 700 °C seems to be due to the increase in crystallinity. However, the following progressive decrease its relative height associated with a broadening in the PO_4^{3-} stretching band at 1041 cm^{-1} with increasing sintering temperature seems to be due to the incorporation of Ti ions into maturing HA crystal structure thus increasing the disorderness and/or the contribution of dehydration of the structural water.[45,46]

The bands at 660 cm^{-1}, 790 cm^{-1}, and 885 cm^{-1} are not characteristic bands of pure HA. Therefore it is supposed that these bands should associate with the presence of Ti ions in HA structure based on the results provided by Chernorukov et al. who observed similar strong bands at around 725–800 cm^{-1}. Therefore these bands were attributed to Ti–O vibrations in –Ti–O–Ti–O– chains.[53] Ribeiro et al. also observed very similar bands in the same range[46] and assigned the band at 790 cm^{-1} to the presence of Ti–O bonds. However, they attained the band at 875 cm^{-1} to a possible pyrophosphate group vibrations.[54,55] The bands at 2300 cm^{-1} may be due to the reaction observed between 1100 °C and 1300 °C.

There are different proposal in the literature for possible Ti substitution mechanisms in HA structure. Among them, Anmin et al. reported that the divalent Ca^{2+} ($r_{Ca^{2+}} = 0.075$ nm) cations should be substituted by quadrivalent ions Ti^{4+} ($r_{Ti^{4+}} = 0.064$ nm) in Ti modified HA structure and therefore the lattice parameters and thus cell volume decreased. Consequently,

Table 3
Lattice parameters and lattice volumes of HA and Ti-doped HA structures

Sample	Temperature	Hexagonal lattice parameters a and c and differences Δa and Δc							
		a	Δa	a^b	Δa^b	c	Δc	c^b	Δc^b
HA	HA	9.427	0	–	–	6.888	0	–	–
	900	9.411	−0.016	9.411	−0.016	6.878	−0.013	6.875	−0.013
C2	1100	9.419	−0.008	9.383	−0.044	6.889	−0.010	6.863	−0.025
	1300	9.411	−0.016	9.386	−0.041	6.882	−0.001	6.872	−0.016
C5	Not determined due to XRD data[a]								
	900	9.411	−0.016	9.411	−0.016	6.882	−0.006	6.882	−0.006
P2	1100	9.425	−0.002	9.400	−0.027	6.881	−0.007	6.868	−0.020
	1300	9.408	−0.019	9.381	−0.046	6.883	−0.005	6.864	−0.024
	900	9.419	−0.008	9.419	−0.008	6.860	−0.028	6.860	−0.028
P5	1100	9.425	−0.002	9.386	−0.041	6.881	−0.007	6.855	−0.033
	1300	9.422	−0.005	9.389	−0.038	6.886	−0.002	6.870	−0.018

Sample	Temperature	Unit cell volumes (V) and differences (ΔV)			
		V	ΔV	V^b	ΔV^b
HA	HA	612.13	0	–	–
	900	608.89	−3.22	608.89	−3.22
C2	1100	610.19	−1.92	604.22	−7.90
	1300	610.13	−1.98	605.40	−6.72
C5	Not determined due to XRD data[a]				
	900	609.51	−2.60	609.51	−2.60
P2	1100	611.24	−0.88	606.85	−5.26
	1300	609.21	−2.90	604.05	−8.07
	900	608.60	−3.52	608.60	−3.52
P5	1100	611.24	−0.88	603.90	−8.22
	1300	611.29	−0.82	605.61	−6.51

[a] The lattice parameters of C5 were not determined due to the high amount of HA decomposition from XRD data.
[b] Calculated from lower intensity pattern in superimposed XRD data.

lattice disorder increased with the increasing of Ti content. The induced lattice disorder may provoke microscopic stresses in HA matrix which can lower the required energy for the dehydration and respected decomposition of its structure. Therefore, the sinterability of HA compacts decreased with increasing the Ti concentration in its structure. It may be this lattice disorder greatly inhibiting the crystallization and making difficult to obtain high crystallinity in HA modified with Ti^{4+}.[43]

On the other hand, Wakamura et al. suggested that Ti ions may be substituted into Ca^{2+} positions in the form of divalent ion complexes, such as $[Ti(OH)_2]^{2+}$ or $[Ti(HPO_4)]^{2+}$, to provide a charge balance in HA lattice.[44] However, they did not make any structural analysis on sintered materials to evaluate the stability of these divalent ion groups with increasing temperature. As the FT-IR results in Fig. 10 shows, the crystallinity of C2 decreased above 900 °C. This may be associated with the lost of OH^- group in $[Ti(OH)_2]^{2+}$ if this ion complex had substituted to Ca^{2+} positions during precipitation. However, the sizes of the proposed Ti-based ion complexes seem to be considerably larger than the site available for Ca ions. Obviously more researches are needed to understand the substitution mechanisms.

It is also plausible that a titanate group can substitute into the location of phosphate group as proposed by Ribeiro et al. Substitution mechanism was described by the following model satisfying appropriate charge balance[46]:

$$Ca_{10}(PO_4)_6(OH)_2\,(\text{solid}) + x{TiO_4}^{4-}\,(\text{aq.}) \Rightarrow Ca_{10}(PO_4)_{6-x}(TiO_4)_x(OH)_{2-x}\,(\text{aq.}) + x{PO_4}^{3-x}\,(\text{aq.}) + x{OH}^-\,(\text{aq.}) \quad (3)$$

They also suggested a possible reaction for the formation of an apatitic structure with a dissolution and precipitation mechanism and they proposed the following chemical formula for this apatitic structure:

$$6{H_2PO_4}^-\,(\text{aq.}) + 5{Ti}^{4+}\,(\text{aq.}) + 2H_2O \Rightarrow 3Ti_5(PO_4)_6(OH)_2\,(\text{solid}) + 14{H}^+\,(\text{aq.}) \quad (4)$$

Although reaction kinetics between HA and $CaTiO_3$ or between TCP and $CaTiO_3$ powders can be mainly affected by the homogeneity of the powder mixture, grain size of the components influencing the diffusion distance between atomic/ionic species, the results obtained from Ti doped samples and composites were quite parallel. For instance, as the XRD patterns of the HC showed similar results to C2, P2 and P5, some amount of HA dissociated to α-TCP at 1100 °C; and this phase completely

disappeared at 1300 °C. On the other hand, TC composite showed no reaction between TCP and $CaTiO_3$ at 1100 °C and 1300 °C, other than a partial transformation of the β-TCP to α-TCP at 1300 °C. In this manner, TC behaved similar to C5.

However, no new peak could be identified in XRD results, which can be assigned to a possible reaction byproduct. As evidence, a new FT-IR band appeared at 2300 cm^{-1} upon sintering the C2 at 1300 °C (Fig. 10) may be considered as an indication for the structural changes caused by this reaction in between 1100 °C and 1300 °C. To the best of our knowledge, this reaction observed in this study has not been demonstrated by other authors.

Two possible mechanisms may be proposed to explain this reaction; (a) the present HA may have provided a surface for nucleation and growth of new apatitic structure formed with the reaction of α-TCP and $CaTiO_3$. Due to its apatitic nature, its XRD peaks may be hindered behind the hydroxylapatite peaks; (b) the reaction product is rather amorphous and therefore, does not have observable XRD peaks.

In the first, TCP and $CaTiO_3$ may react and form a kind of apatitic structure on the HA surface. Keeping in mind that according to our results, the reaction temperature was in between 1100 °C and 1300 °C, structural water for apatite formula is less likely to be provided from air at these temperature levels. Therefore, the following model, for the first time, may be proposed for the formation of a possible apatitic structure on the surface provided with the existing HA phase:

$$CaTiO_3 \Rightarrow Ca^{2+} + {TiO_3}^{2-}$$

$$3Ca_3(PO_4)_2 + CaTiO_3 \Rightarrow Ca_{10}(PO_4)_6(TiO_3) \quad (5)$$

Obviously, in order for ${TiO_3}^{2-}$ ion to substitute into OH sites, the space left by OH ions should be suitable as well as charge neutrality should be maintained. Taking into account that the distance between Ca(II) and O in OH is about 0.238 nm; the distance between Ca(II) and H in OH is about 0.269 nm.[15] So the radius of a minimum spherical space in O column of a loosely packed HA can be considered as 0.238 nm. On the other hand, if the length of Ti–O bond is considered as 0.18 nm, the top angle of O–Ti–O trigonal as about 90°,[56] the radius of Ti^{4+} as 0.064 nm and the radius of O^{2-} as 0.14 nm, then the minimum radius of the spherical space that would be filled by ${TiO_3}^{2-}$ ion can be considered roughly as 0.16 nm. So, it seems to be plausible that ${TiO_3}^{2-}$ group could squeeze in an OH site. Another possibility would be the ${TiO_2}^{1-}$ ion instead of ${TiO_3}^{2-}$, which has one net negative charge if its Ti species is in three-valent state.

In the second, HA and $CaTiO_3$ may react with each other in the expense of both phases. The following model, also for the first time, can be proposed for the respected reaction:

$$Ca_{10}(PO_4)_6(OH)_2\,(\text{solid}) + CaTiO_3 + xO_2 \Rightarrow Ca_{10}(PO_4)_5(TiO_4)(OH)_2 + Ca_2P_4O_9 \quad (6)$$

Since the melting temperature of calcium pyrophosphate is about 1230 °C, this phase might have melted during sintering.[57] After solidification, this phase might have not crystallized again and therefore formed a glassy phase, similar to the reaction proposed in $HA/LaPO_4$ systems.[58] This may be the reason why it could not be detected in X-ray diffraction results. This model can also explain why α-TCP and $CaTiO_3$ did not react in the absence of HA in C5 and TC composite, however, it cannot explain how α-TCP disappeared.

SEM analyses revealed that for each of the Ti substituted HA, except C5, sub-micrometer grain sizes were measured. So it can be inferred that Ti incorporation into HA structure yielded a decrease in the grain size. As previously demonstrated, the Ti concentration increased in the compacts of interest, α-TCP and $CaTiO_3$ phases became more stable up to 1100 °C. However, as the concentration of these phases increased, so did porosity. Therefore it may also be accepted that the existence of Ti in the structure promoted the dehydration of HA phase which may be responsible for diminishing the densification behavior. The formation of pores in the compacts with increased amount of Ti may be due to the dehydration of hydroxyl-groups (and associated saturated water) from HA leading to the formation of α-TCP as observed in C5 with the following proposed reaction:

$$Ca_{10}(PO_4)_6(OH)_2 + Ti^{4+} \Rightarrow 3Ca_3(PO_4)_2 + CaTiO_3 + H_2O \quad (7)$$

5. Conclusion

This study demonstrated that during the synthesis of Ti substituted HA, two different apatitic structures formed in the precipitating medium. These phases crystallized above 900 °C, and became observable in XRD analysis. The one with the higher intensity may belong to Ti ion substituted HA lattice. However the one with the lower intensity may belong to one in which Ti ions dominated in its crystal formulation. The incorporation of the Ti ions into the HA led to the shrinkage of the unit lattice volume.

Ti incorporation caused a decrease in grain size of HA. However, Ti ions beyond certain limit promoted the decomposition of HA phase and formation of porosity. Thus α-$Ca_3(PO_4)_2$ and $CaTiO_3$ phases became stable.

A reaction involving HA, α-$Ca_3(PO_4)_2$ and $CaTiO_3$ was observed, for the first time, in Ti substituted samples and $HA/CaTiO_3$ composites upon sintering between 1100 °C and 1300 °C. In the absence of HA or below some critical volume ratio, this reaction was not observed and both α-$Ca_3(PO_4)_2$ and $CaTiO_3$ phases stayed stable.

Acknowledgements

This work is partially supported by the Scientific & Technological Research Council of Turkey-BAYG program. The author wish to express his gratitude to Prof. John W. Halloran (Department of Materials Science and Engineering, the University of Michigan, Ann Arbor, USA) for his valuable contributions.

References

1. De Groot, K., Bioceramics consisting of calcium–phosphate salts. *Biomaterials*, 1980, **1**, 47.

2. Jarcho, M., Calcium phosphate ceramics as hard tissue replacements. *Clin. Orthop.*, 1981, **157**, 259.
3. LeGeros, R. Z., Calcium phosphate materials in restorative dentistry: a review. *Adv. Dent. Res.*, 1988, **2**, 164.
4. Daculsi, G., Passuti, N. and Martin, S., Macroporous calcium phosphate ceramic for long bone surgery inhuman and dogs: clinical and histological study. *J. Biomed. Mater. Res.*, 1990, **24**, 379.
5. LeGeros, R. Z., Apatite in biological systems. *Prog. Cryst. Growth Charact.*, 1981, **4**, 1.
6. Narasaraju, T. S. B. and Phebe, D. E., Some physiochemical aspects of hydroxylapatite. *J. Mater. Sci.*, 1996, **31**, 1.
7. Itokazu, M., Yang, W., Aoki, T. and Kato, N., Synthesis of antibiotic-loaded interporous hydroxyapatite blocks by vacuum method and in vitro drug release testing. *Biomaterials*, 1998, **19**, 817.
8. Kenny, S. M. and Buggy, M., Bone cements and fillers: a review. *J. Mater. Sci.: Mater. Med.*, 2003, **14**, 923.
9. Niwa, M., Sato, T., Li, W., Aoki, H., Aoki, H. and Daisaku, T., Polishing and whitening properties of toothpaste containing hydroxylapatite. *J. Mater. Sci.: Mater. Med.*, 2001, **12**, 277.
10. Riman, R. R., Suchanek, W. L., Byrappa, K., Chen, C. W., Shuk, P. and Oakes, C. S., Solution synthesis of hydroxyapatite designer particulates. *Solid State Ionics*, 2002, **151**, 393.
11. Takashima, S., Hayakawa, S., Ohtsuki, C. and Osaka, A., Adsorption of proteins by calcium phosphate with varied Ca to P ratios. *Bioceramics*, 1996, **9**, 217.
12. Takashima, S., Kusudo, Y., Takemoto, S., Tsuru, K., Hayakawa, S. and Osaka, A., Synthesis of carbonate-hydroxyapatite and selective adsorption activity against specific pathogenic substances. *Bioceramics*, 2002, **14**, 175.
13. Hayakawa, S., Kusudo, Y., Takemoto, S., Tsuru, K. and Osaka, A., Hydroxy-carbonate apatite, blood compatibility and adsorption of specific pathogenic proteins. *Bioceram.: Mater. Appl. IV*, 2003, **147**, 111.
14. Takemoto, S., Kusudo, U., Tsuru, K., Hayakawa, S., Osaka, A. and Takashima, S., Selective protein adsorption and blood compatibility of hydroxy-carbonate apatites. *J. Biomed. Mater. Res.*, 2004, **69A**, 544.
15. Kay, M. I., Young, R. A. and Posner, A. S., Crystal structure of hydroxylapatite. *Nature*, 1964, **204**, 1050.
16. Elliot, J. C., *Structure and Chemistry of the Apatites and other Calcium Orthophosphates*. Elsevier, Amsterdam, 1994.
17. Senger, B., Bres, E. E., Hutchison, J. L., Voegel, J. C. and Frank, R. M., Ballistic damages induced by electrons in hydroxyapatite (ohap). *Philos. Mag.*, 1992, **65**, 665.
18. Chu, C., Lin, P., Dong, Y., Xue, X., Zhu, J. and Yin, Z., Fabrication and characterization of hydroxylapatite reinforced with 20 vol% particles for use as hard tissue replacement. *J. Mater. Sci.: Mater. Med.*, 2002, **13**, 985.
19. Garcia, R. and Doremus, R. H., Electron microscopy of the bone implant interface from a human dental implant. *J. Mater. Sci.: Mater. Med.*, 1992, **27**, 285.
20. Gaines, R. V., Skinner, H. C. W., Foord, E. F., Mason, B. and Rosenzweig, A., *Dana's New Mineralogy*. Wiley, New York, 1997, p. 854.
21. Ergun, C., Webster, T. J., Bizios, R. and Doremus, R. H., Hydroxylapatite with substituted magnesium, zinc, cadmium, and yttrium. Part I. Mechanisms of osteoblast adhesion. *J. Biomed. Mater. Res.*, 2002, **59**, 305.
22. Sinkova, L. A., Ivanov, V. I. and Filippov, L. V., An experimental study of the incorporation of rare-earth elements in hydroxylapatite. *Geochem. Int.*, 1968, **5**, 289–298 [translated from Geokhimiya 1968, 3, 304].
23. Nelson, D. G. A. and Featherstone, J. D. B., Preparation, analysis, and characterization of carbonated apatites. *Calcified Tissue Int.*, 1982, **34**, 69.
24. Vignoles, M., Bonel, G. and Young, R. A., Occurrence of nitrogenous species in precipitated b-type carbonated hydroxylapatites. *Calcified Tissue Int.*, 1987, **40**, 64.
25. Vignoles, M., Bonel, G., Holcomb, D. W. and Young, R. A., Influence of preparation conditions on the composition of type-b carbonated hydroxylapatite and on the localization of the carbonate ions. *Calcified Tissue Int.*, 1988, **43**, 33.
26. Gibson, I. R. and Bonfield, W., Preparation and characterization of magnesium carbonate co-substituted hydroxylapatites. *J. Mater. Sci.: Mater. Med.*, 2002, **13**, 685.
27. Tampieri, A., Celotti, G., Sprio, S. and Mingazzini, C., Characteristics of synthetic hydroxylapatites and attempts to improve their thermal stability. *Mater. Chem. Phys.*, 2000, **64**, 54.
28. Kim, H. W., Noh, Y. J., Koh, Y. H., Kim, H. E. and Kim, H. M., Effect of CaF_2 on densification and properties of hydroxyapatite–zirconia composites for biomedical applications. *Biomaterials*, 2002, **23**, 4113.
29. Kijkowska, R., Lin, S. and LeGeros, R. Z., Physico-chemical and thermal properties of chlor-, fluor- and hydroxyapatites. *Key Eng. Mater.*, 2002, **218**(2), 31–34.
30. Rameshbabu, N., Sampath Kumar, T. S., Prabhakar, T. G., Sastry, V. S., Murty, K. V. G. K. and Rao, K. P., Antibacterial nanosized silver substituted hydroxyapatite: synthesis and characterization. *J. Biomed. Mater. Res.*, 2007, **80A**, 581.
31. Thurman, R. B. and Gerba, C. P., The molecular mechanisms of copper and silver ion disinfection of bacteria and viruses. *CRC Crit. Rev. Environ. Control*, 1989, **18**, 295.
32. Kim, T. N., Feng, Q. L., Kim, J. O., Wu, J., Wang, H., Chen, G. C. *et al.*, Antimicrobial effects of metal ions (Ag^+, Cu^{2+}, Zn^{2+}) in hydroxyapatite. *J. Mater. Sci.: Mater. Med.*, 1998, **9**, 129.
33. Thian, E. S., Huang, J., Best, S. M., Barber, Z. H. and Bonfield, W., Silicon-substituted hydroxyapatite thin films: effect of annealing temperature on coating stability and bioactivity. *J. Biomed. Mater. Res.*, 2006, **78A**, 121.
34. Chappell, H. F. and Bristowe, P. D., Desnsity functional calculation of the properties of silicon-substituted hydroxyapatite. *J. Mater. Sci.: Mater. Med.*, 2007, **18**, 829.
35. Fujii, E., Ohkubo, M., Tsuru, K., Hayakawa, S., Osaka, A., Kawabata, K. *et al.*, Selective protein adsorption property and characterization of nano-crystalline zinc-containing hydroxylapatite. *Acta Biomater.*, 2006, **2**, 69.
36. Webster, T. J., Ergun, C., Doremus, R. H. and Bizios, R., Hydroxylapatite with substituted magnesium, zinc, cadmium, and yttrium. Part II. Mechanisms of osteoblast adhesion. *J. Biomed. Mater. Res.*, 2002, **59**, 312.
37. Wakamura, M., Kandori, K. and Ishikawa, T., Influence of chromium(III) on the formation of calcium hydroxyapatite. *Polyhedron*, 1997, **16**, 2047.
38. Evis, Z., Al^+-doped nano-hydroxyapatites and their sintering characteristics. *J. Ceram. Soc. Jpn.*, 2006, **114**, 1335.
39. Wakamura, M., Kandori, K. and Ishikawa, T., Surface structure and composition of calcium hydroxyapatites substituted with Al(III), La(III) and Fe(III) ions. *Colloids Surf.*, 2000, **164**, 297.
40. Ternane, R., Trabelsi-Ayedi, M., Kbirariguib, N. and Piriou, B., Luminescent properties of Eu^{3+} in calcium hydroxyapatite. *J. Lumin.*, 1999, **81**, 165.
41. Feng, Z., Liao, Y. and Ye, M., Synthesis and structure of cerium-substituted hydroxyapatite. *J. Mater. Sci.: Mater. Med.*, 2005, **16**, 417.
42. Ergun, C., Doremus, R. H. and Lanford, W. A., Hydroxylapatite–titanium: interfacial reactions. *J. Biomed. Mater. Res.*, 2003, **63A**, 336.
43. Anmin, H., Ming, L., Chengkang, C. and Dali, M., Preparation and characterization of a titanium-substituted hydroxyapatite photocatalyst. *J. Mol. Catal. A: Chem.*, 2007, **267**, 79.
44. Wakamura, M., Hashimoto, K. and Watanabe, T., Photocatalysis by calcium hydroxyapatite modified with Ti(IV): albumin decomposition and bactericidal effect. *Langmuir*, 2003, **19**, 3438.
45. Hu, C., Guo, J., Qu, J. and Hu, X., Efficient destruction of bacteria with Ti(IV) and antibacterial ions in co-substituted hydroxyapatite film. *Appl. Catal. B: Environ.*, 2007, **73**, 345.
46. Ribeiro, C. C., Gibson, I. and Barbosa, M. A., The uptake of titanium ions by hydroxyapatite particles—structural changes and possible mechanisms. *Biomaterials*, 2006, **27**, 1749.
47. Ergun, C., Liu, H., Webster, T. J. and Halloran, J. W., Increased osteoblast adhesion on nanograined hydroxyapatite and tricalcium phosphate containing calcium titanate. *J. Biomed. Mater. Res.*, 2007, **80A**, 990.
48. Hillyard, J. E., Estimating the grain size by the intercept method. *Met. Prog.*, 1964, **85/86**, 99.
49. Hillyard, J. E. and Cahn, J. W., An evaluation of procedures in quantitative metallography for volume fraction analysis. *Trans. Metall. Soc. AIME*, 1961, **221**, 344.
50. Evis, Z., Ergun, C. and Doremus, R. H., Hydroxylapatite–zirconia composites: thermal stability of phases and sinterability as related to the $CaO–ZrO_2$ phase diagram. *J. Mater. Sci.*, 2005, **40**, 1127.

51. Ducheyne, P. and Radin, S., Calcium phosphate ceramic coatings on porous titanium: effect of structure and composition on electrophoretic deposition, vacuum sintering and in vitro dissolution. *Biomaterials*, 1990, **11**, 244.
52. Zeng, H. and Lacefield, W. R., XPS, EDX and FTIR analysis of pulsed laser deposited calcium phosphate bioceramics coatings: the effects of various process parameters. *Biomaterials*, 2000, **21**, 23.
53. Chernorukov, N. G., Korshunov, I. A. and Zhuk, M. I., Hydro-*ortho*-derivatives of titanium of composition $Ti(OH)PO_4$ and $Ti(OH)AsO_4$. *Russ. J. Inorg. Chem.*, 1982, **27**, 1728.
54. Jazouli, A. E. L., Krimi, S., Manoun, B., Chaminade, J. P., Gravereau, P. and De Waal, D., Preparation and structural characterization of two new titanium phosphates $NaCa_{0.5}Ti(PO_4)_3$ and $Ni_{0.5}TiOPO_4$. *Ann. Chim. Sci. Mater.*, 1998, **23**, 7.
55. Bamberger, C. E., Begun, G. B. and Cavin, O. B., Synthesis and characterization of sodium-titanium phosphates, $Na_4(TiO)(PO_4)_2$, $Na(TiO)PO_4$ and $NaTi_2(PO_4)_3$. *J. Solid State Chem.*, 1988, **73**, 317.
56. Hayashi, K., Murakami, H. and Nomiya, K., Novel T–O–T bonding species constructed in a metal oxide cluster. *Dalton Trans.*, 2005, **23**, 3751.
57. Bian, J. J., Kim, D. W. and Hong, K. S., Phase transformation and sintering behavior of $Ca_2P_2O_7$. *Mater. Lett.*, 2004, **58**, 374.
58. Ergun, C., Synthesis and characterization of machinable calcium phosphate/lanthanum phosphate composites. *J. Mater. Process. Tech.*, 2008, **199**, 178.